

## Techniques for Positional Measurements of Telescopic Meteor TV Images

Yu. M. Gorbanev\*, A. V. Golubaev, V. V. Zhukov, I. I. Kimakovskaya, S. R. Kimakovskiy,  
E. F. Knyazkova, S. V. Podlesnyak, L. A. Sarest, I. A. Stogneeveva, and V. A. Shestopalov

*Astronomical Institute, Odessa National University, Odessa, Ukraine*

\* E-mail: skydust@tm.odessa.ua

Received March 1, 2007

**Abstract**—We present the results of our positional reduction of the observational material obtained using a meteor patrol based on a Schmidt telescope and a TV CCD detector. More than 1000 telescopic meteors were recorded in three years of meteor patrolling. Techniques for the cataloging and positional reduction of 3050 TV images with meteor trails are described. We have developed a technique for measuring the images of reference stars to determine the rectangular coordinates in the image frame. We discuss the achieved accuracy of determining the equatorial coordinates of reference and check stars by Turner's method (of the order of a few arcseconds). We have developed software that allows the rectangular coordinates of meteor trajectory points to be determined after the meteor image reduction. These coordinates are used to determine the equatorial coordinates of the poles of the great circles of meteor trajectories (the angular length is not less than  $15'$  with an accuracy of at least  $4'$ ). We consider the possibility of using Stanyukovich's method to determine the equatorial coordinates of radiants for non-basis meteor observations. The accuracy of determining the radiant coordinates has been estimated to be  $4'–5'$ . Prospects for obtaining the kinematic characteristics of meteor particles are discussed.

PACS numbers: 96.30.Za; 91.65.Sn; 94.20.Xa; 91.67.gn-in

DOI: 10.1134/S003809460801005X

### INTRODUCTION

Many problems of meteor astronomy to determine the kinematic and physical characteristics of meteor events require accurate positional measurements. Positional measurements are based on the observations obtained by various methods: visual, photographic, TV, or radar. Collectively, they encompass a wide range of masses and velocities of recorded meteor particles. The determination accuracies can differ by several orders of magnitude, depending on the physical properties of the recorded meteor events, recording conditions, and capabilities of the observing technique.

One of the objectives of investigating the spatial distribution of meteor-produced particles is to determine their radiants.

Martynenko et al. (1978) claimed that the accuracy of determining the radiants of meteors in visual observations was  $0.2^\circ–0.5^\circ$ . Such results can be obtained only by groups of experienced observers that carefully follow a rigorous observing technique. Otherwise, the accuracy will be not better than  $1^\circ$ .

Kashcheev and Lebedinets (1961) concluded that the radar determinations of the radiant coordinates for individual meteors could be made with an accuracy of  $\pm 2.5^\circ$ .

To determine the radiant coordinates when using the photographic or TV method, one measures meteor tra-

jectory points and then calculates the corresponding coordinates of the poles of the great circles. The accuracy of measuring individual meteor trajectory points will determine the accuracy of calculating the pole and radiant coordinates.

Kozak (2002) analyzed the methods and accuracies of determining the equatorial coordinates in the case of digital reduction of meteor TV observations. For an instrument with a Jupiter-3 short-focus lens ( $F = 50$  mm,  $D : F = 1 : 1.5$ ) and an image size of  $352 \times 288$  pixels, the angular size of one pixel is about  $4'$  and the minimum possible error in the equatorial coordinates of meteor trajectory points is  $1.5'–3.5'$ .

The angular accuracy of measuring a point in a photograph taken with Zonar, Industar-7, and Ksenon short-focus lenses is  $\pm 18''$  at a mean measurement error of  $5 \times 10^{-3}$  mm. (Katasev, 1966).

According to Simakina (1968), the coordinates of points in the photographic image of a meteor were determined, on average, with an error of the order of  $\pm 5''–8''$  (Odessa),  $\pm 10''–20''$  (Dushanbe), and  $\pm 10''–20''$  (Harvard). The arcsecond accuracy stems from the fact that astrocameras with a focal length of at least  $\sim 250$  mm were used during the meteor patrolling and a photographic emulsion served as the detector.

The following dilemma arises when planning and implementing a meteor patrol: increasing the accuracy

of the meteor image measurements requires increasing the focal length of the astrocamera or telescope. This entails a decrease in the working field, which affects negatively the observed meteor statistics and the length of the meteor trajectory recorded by the detector.

Therefore, there exists a great variety in the equipment of meteor patrols, depending on the problems solved with the developed instrument.

When implementing our meteor patrol, we have been oriented to studying faint meteor events that have been observed only by the telescopic and radar methods so far. Combining the telescopic method with the use of a panoramic TV detector as the recorder, we were able to record the images of faint meteors with a high spatial resolution. Such meteors have been recorded so far by chance in the images obtained with telescopes at long exposures in the form of streaks crossing the image from edge to edge. The meteor timing was possible only with an accuracy equal to the exposure time.

The meteor patrol at the Kryzhanovka observing station of the Odessa Astronomical Observatory was described previously (Gorbanev et al., 2006). The patrol was installed on the APSH-4 equatorial mounting and equipped with a Schmidt telescope (the correction plate diameter is 170 mm and the mirror diameter is 300 mm). The focal length of the telescope is 534 mm. A high-sensitivity Watec-LCL-902K video camera operating in the PAL TV standard (25 frames per second) is used as the detector. This video camera with the above parameters of the telescope allows a  $36' \times 48'$  sky field to be selected, while the angular size of a single image pixel is  $\sim 4''$ . Stars to  $+12.8^m$  in the  $V$  photometric band can be recorded at the telescope's focus.

#### OBSERVATIONAL MATERIAL. THE METEOR DATABASE

After a night of meteor patrolling, whose technique was described previously (Gorbanev et al., 2006), movies consisting of 50 frames before and after the meteor event and frames with meteor trails are entered into the database. This procedure is performed using our *AVICutter 1.02* software, which directly cuts out frames with meteor trails from the movie and produces images for even and odd frame lines.

In what follows, we will italicize our software for the convenience of perception. We will also call the even and odd half-frames the images composed of the even and odd frame lines, respectively.

Additionally, 50 frames are summed before the meteor event: the mean intensity is calculated for each point from the intensities for the same point based on all 50 frames. We will designate the image obtained in this way a *summed frame*. Recall that frame summation allows the limiting magnitude to be increased approximately by one or two magnitudes. Using 50 movie frames (@2 s) for the summation was justified in more detail previously (Gorbanev et al., 2006). The summed

images produced in this way are subsequently used for positional and photometric measurements, although individual movie frames with exposures of 20 or 40 ms are also suitable for this purpose.

The mean intensity and the rms deviation are calculated separately for each image pixel based on the entire series of 50 frames preceding the meteor event. Subsequently, these data are used to calculate the background intensities at the points where the meteor trail was recorded. We will call the files with background intensity data *background maps*.

Each movie with the image of an object is identified by the following data in its name: the object number in a 15-min patrolling session over the observing night, the object type (a meteor, a comet, a satellite, etc.), the date (day, month, year), and the number of the 15-min session itself. This identification allows the search for meteors in the database to be rapidly conducted. The characteristic view of an individual frame with a meteor trail is presented in Fig. 1a; as was pointed out above, the size of the working field is  $36' \times 48'$ .

Each meteor is entered into the catalog where a serial number is assigned to it. In addition, the date of observation, the AVI movie name, the observer code, the movie recording start time (UTC), the guide star from a reference catalog (SAO, Tycho-2, Hipparcos, or USNO-A2), and the equatorial coordinates of the image center are entered into the catalog.

Subsequently, a primary reduction of the observational material is performed: frames with meteor trails are selected from the movie and a catalog of meteor images with the numbering of individual frames for each event is compiled. The catalog of star fields is also supplemented by the *summed* frames.

All stars in the images are identified and numbered and are then entered into a summary catalog: the star catalog name, equatorial coordinates, magnitudes, color indices, spectral types, etc. The compiled catalogs allow these data to be subsequently used to determine the equatorial coordinates and apparent magnitudes of meteors.

Initially, the images were identified using well-known software, but much time was spent on this identification due to the specifics of our observational material. At present, the development of the *PSF 1.01* software, which allows an online identification to be performed in a few seconds by the guide star number in the connected star catalog, has been finished.

The preliminary measurements are entered into the database where the measured magnitudes of meteors and reference stars are stored and a working map with the rectangular coordinates of stars in the image frame, all meteor streaks, flight directions, etc. is produced (Fig. 1b). The reduced meteor images are accumulated in a photometric database. More than 1000 meteors had been recorded by March 2007 at a total meteor patrolling time of about 2000 h. The total number of images with meteor trails is 3050.

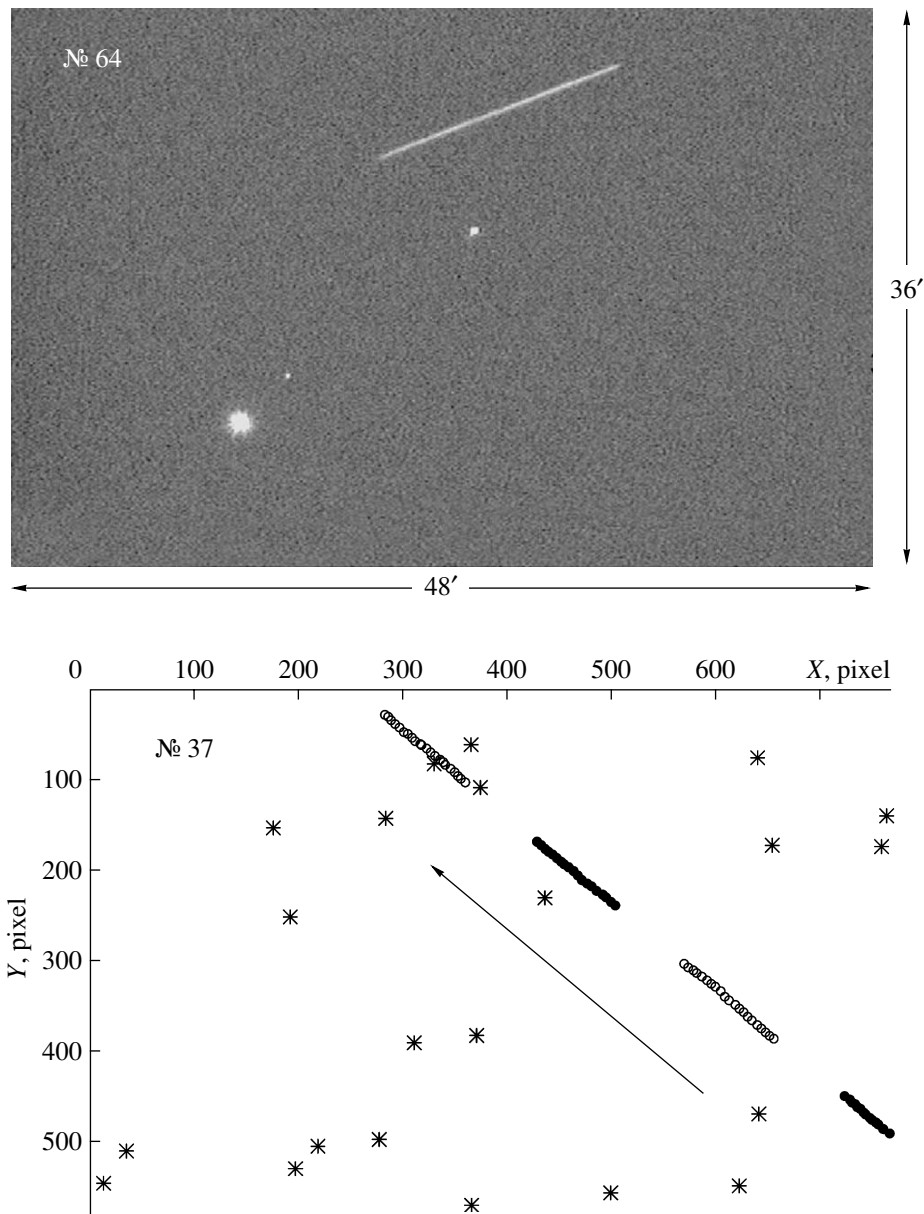


Fig. 1. Typical meteor image and a reduction card from the database.

#### POSITIONAL MEASUREMENTS OF STARS

Reference stars with known equatorial coordinates are used for positional measurements. The accuracy of determining the meteor trajectory coordinates depends on the number of stars in the image. Figure 2 presents a histogram of the number distribution of reference stars in the images obtained using our meteor patrol; the minimum number of reference stars is 10, the distribution maximum is in the range 20–25, and the maximum number is 88. For Turner's method, this number distribution of reference stars is quite acceptable (Mikhailov, 1967).

Measuring the rectangular coordinate of reference stars in the image frame is one of the positional meteor

image reduction steps. There exist many software tools for such measurements. However, since they are used in most cases for star image measurements, while we need to measure meteor images in addition to stars, we developed our own software for these purposes.

To check the measuring technique and our software for proper operation, we performed a simultaneous reduction using the IRIS software (developed by Christian Buil, <http://www.astrosurf.com/buil>, freeware). This software allows astrometric and photometric measurements to be performed using the principles of aperture photometry. The results of the star image reduction using the IRIS software are presented in Behrend et al. (2002).

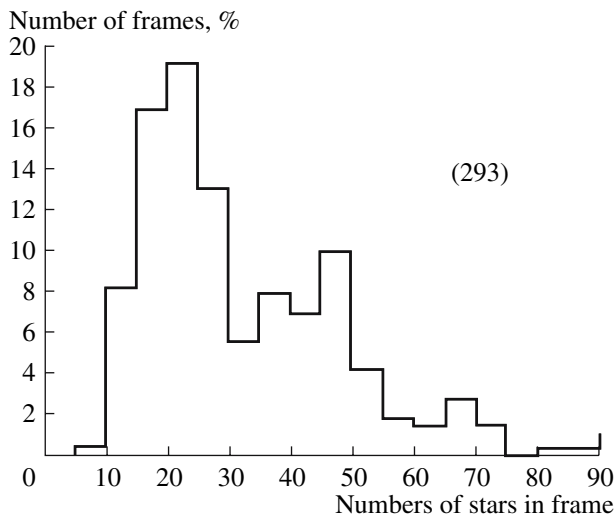


**Fig. 2.** Histogram of the number distribution of reference stars in the images.

According to our technique, in measuring a star image, we first analyze the image and select the points belonging to the star image. For this purpose, we use the intensities of the background pixels around the star image and attribute all of the points with intensities larger than  $3\sigma$  of the background level to the star image.

Subsequently, we search for the photometric image center using the formulas

$$X = \frac{\sum (X_i I_i)}{\sum I_i}; \quad Y = \frac{\sum (Y_i I_i)}{\sum I_i}, \quad (1)$$

where  $X_i$  and  $Y_i$  are the rectangular coordinates of the working pixel, and  $I_i$  is the signal intensity in arbitrary units. Thus, the rectangular coordinates in the image frame are fractional and the following question arises: With what accuracy (in pixels) can we measure the star image? The measurement accuracy can be checked many times by measuring the star images. However, if there exists a systematic error in the technique, then such measurements do not allow the shortcomings to be revealed. To reveal the possible systematic errors, we reduced the same images using our software and IRIS. Figure 3 compares the measurements. The difference between the  $X$  ( $\Delta x$ ) (Fig. 3a) and  $Y$  ( $\Delta y$ ) (Fig. 3b) coordinates and the distance  $\Delta$  between the points (Fig. 3c) for the measurements performed with the two programs show the limiting values of the possible systematic errors. The standard deviations for the  $X$  and  $Y$  coordinates are 0.2 and 0.26, respectively. The mean value for  $\Delta$  is 0.28 at a standard deviation of 0.18 pixel.

The concept of a magnitude equation, which is defined as the relative displacement of the positions of stars with images of different sizes in the plate due to different structures of these images and peculiarities of

their measurements, is used in photographic positional measurements. For TV images with a CCD detector, there also exist measurements for which the deviations reach 0.5–1 pixel, because the star image brightness affects the measurement accuracy. This is illustrated by Fig. 4a, which presents the dependence of the accuracy of measuring the coordinates of check stars on their magnitudes. These data were obtained after the reduction of a series of images with identified reference stars by Turner's method (Mikhailov, 1967; Kramer and Shestak, 1989; Gehrels et al., 1986; Codina et al., 1992) using 6 or 12 constants and then the residuals were calculated for check stars with different magnitudes (in the  $S_V$  band). As we see from the figure, the accuracy of determining the equatorial coordinates for bright stars depends on the magnitude. Stars brighter than  $6^m$  are very unreliable for positional measurements because of the large star image sizes: in the range  $6^m$ – $11^m$ , the positional measurement accuracy is at least  $2''$ . For a third of the stars fainter than  $11^m$ , the positional measurement accuracy increases, because the images of such stars are small and the distortions emerging on CCD array pixels are significant. The background fluctuations also deteriorate the accuracy of measuring the images of stars fainter than  $11^m$ .

Therefore, when reference stars are chosen for positional measurements of the images obtained with our instrument, stars brighter than  $6^m$  should be excluded and stars fainter than  $11^m$  should be used selectively.

Not reference stars, whose residuals characterize the internal accuracy of Turner's method for a given sample, but check stars should be used to estimate the accuracy of our positional measurements. This approach allows the external accuracy of the positional measurements to be determined. To obtain the accuracy for the actual meteor trail recorded in a certain part of the frame (occasionally in the image corner), we use check stars in this region. Figure 4b presents polygons of the error distributions for a sample of reference and check stars based on 86 images (a sample of 1259 stars). For reference stars, the errors do not exceed  $2.0''$  and have a distribution maximum of  $0.7''$ – $0.8''$ . The maximum of the error distribution for check stars is shifted and is more than  $1.0''$ , while the range of values increases to  $5''$ . Thus, for each TV image, the measurement error is calculated using check stars near the meteor trail and gives an idea of the positional accuracy.

#### THE TECHNIQUE FOR POSITIONAL MEASUREMENTS OF METEOR IMAGES

The TV images of meteors differ fundamentally from those of stars from the standpoint of measurement reduction. In contrast to the star image, the meteor image is a streak of a certain length. The accuracy of measuring the coordinates of a point on the meteor trajectory depends on the meteor magnitude, event diffusivity, and image width. The measurement of meteor trajectory points can be divided into two main steps:

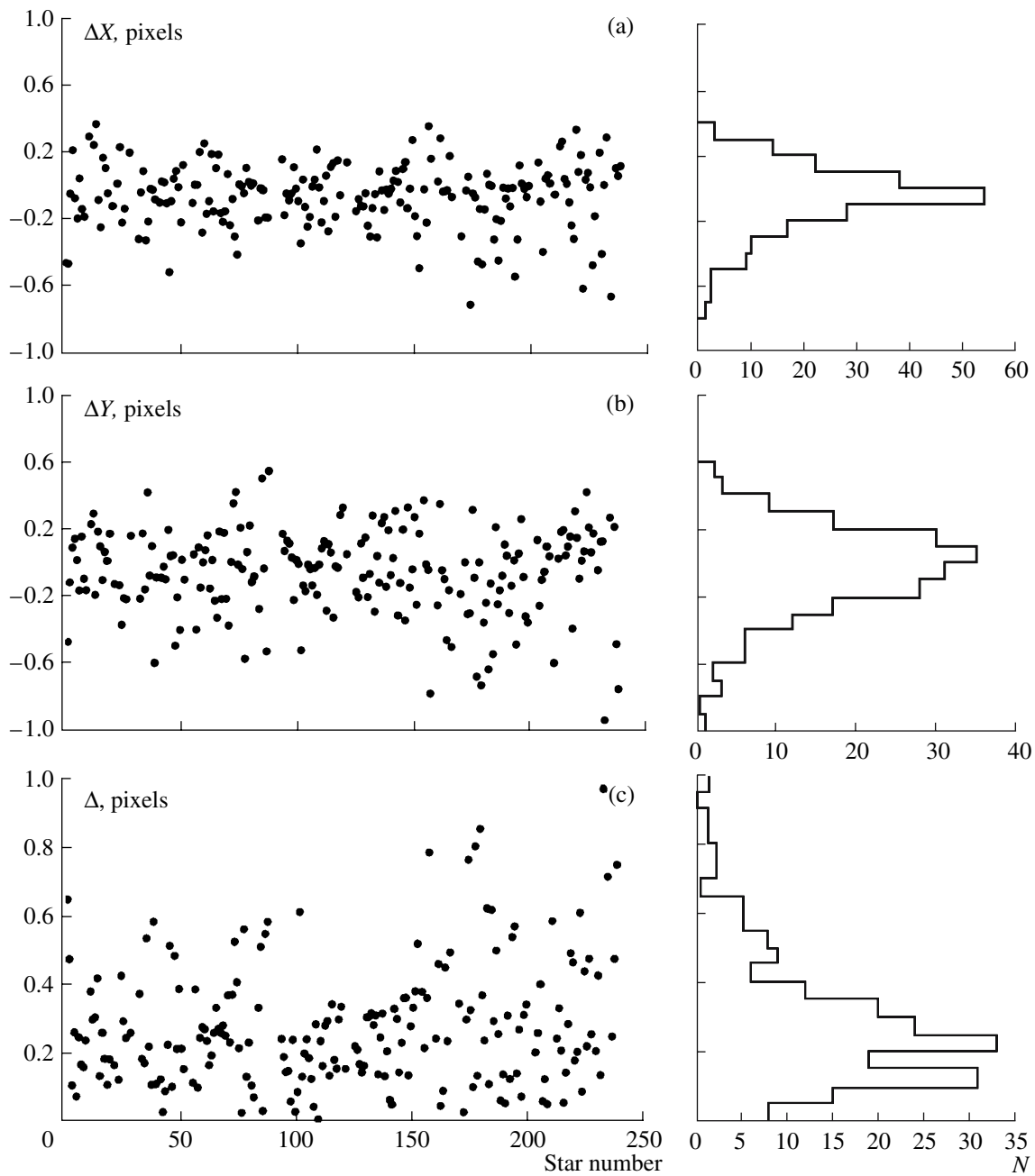


**Fig. 3.** Comparison of the measured rectangular coordinates of star images. The differences in the rectangular coordinates obtained using our software (see the text) and IRIS: (a) in  $X$  coordinate; (b) in  $Y$  coordinate; (c) total distance between the corresponding points. The distributions of differences for each plot are presented in the histogram.

measuring the coordinates of trajectory points and the coordinates of the meteor streak ends. The meteor streak ends will be measured with a lower accuracy, because the meteor image is asymmetric.

We used three independent techniques that we developed for the positional measurements of meteor images.

The first technique is similar to the technique for photographic negative measurements with a measuring instrument. When pointing at the point being measured,

the operator uses either only photometric capabilities of the eye or auxiliary horizontal and vertical scans to adjust the measuring marker. The meteor streak ends are particularly difficult to measure; an example of such measurements is given in Fig. 5a. In this case, the error can reach 3 pixels, depending on the image form (Fig. 5b). Particular difficulties arise when measuring meteor images with tails. In this case, the measurement error increases by a factor of 2 or 3. We use this method only as a preliminary one.

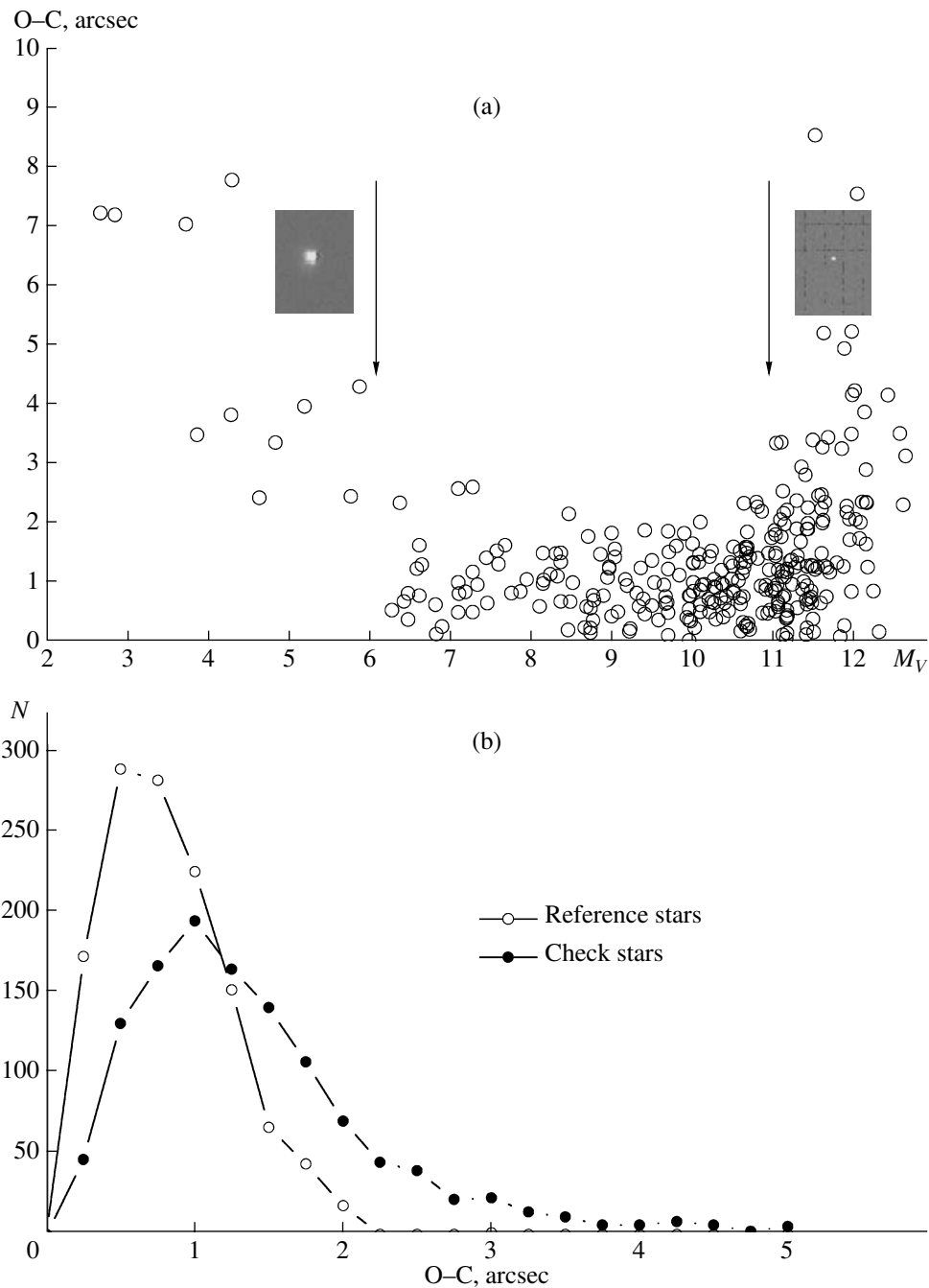


**Fig. 4.** (a) Positional measurement accuracy versus star brightness and (b) polygons of the distribution of residuals for references and check stars.

The second technique is used in an automated measuring system that suggests the following procedures: successive meteor image loading (Fig. 6a; the arrow indicates the flight direction), background intensity determination, meteor image pixel identification (Fig. 6b), and, finally, meteor trajectory determination (Fig. 6c).

Below, we describe the method of obtaining the longitudinal profile of a meteor trajectory image. We tested three alternative variants of calculating the profiles of

meteor images: the profile along the  $X$  axis (hereafter an  $X$  scan); the profile along the  $Y$  axis (hereafter an  $Y$  scan); and the profile along the straight line that specifies the meteor trajectory direction (hereafter an  $L$  scan), the straight line is the meteor image axis. To obtain the  $X$  scan, we split up all images in  $X$  coordinate into  $N$  sectors with width  $dx$ :

$$N = \frac{(X_{\max} - X_{\min})}{dx}. \quad (2)$$

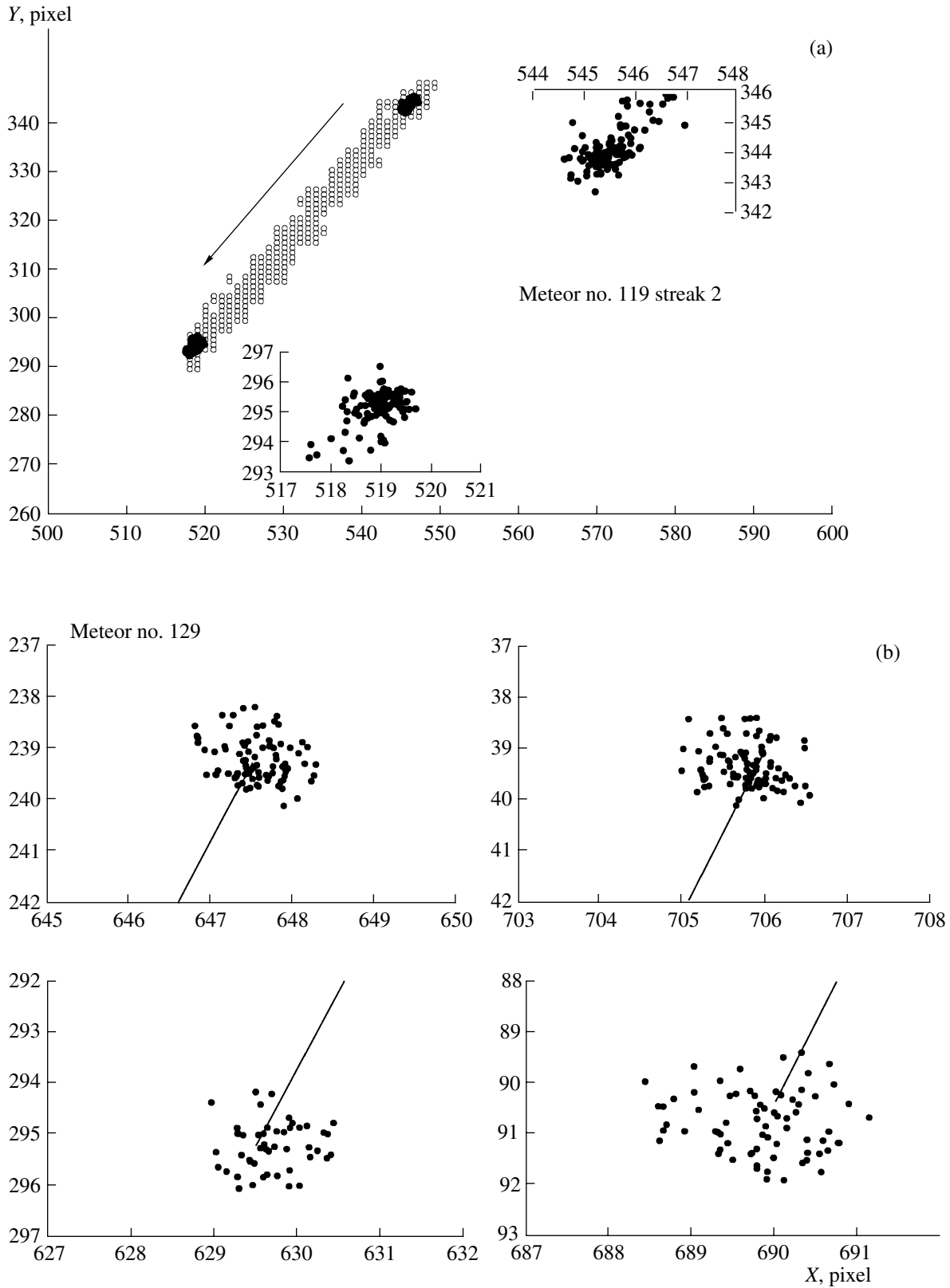


**Fig. 5.** Measurement accuracy for meteor streak images (the rectangular coordinates in the image frame are along the axes; the arrows indicate the meteor particle flight direction): (a) typical example of manually measuring the ends of the meteor streak; (b) examples of manually measuring the ends of various meteor streaks for one meteor.

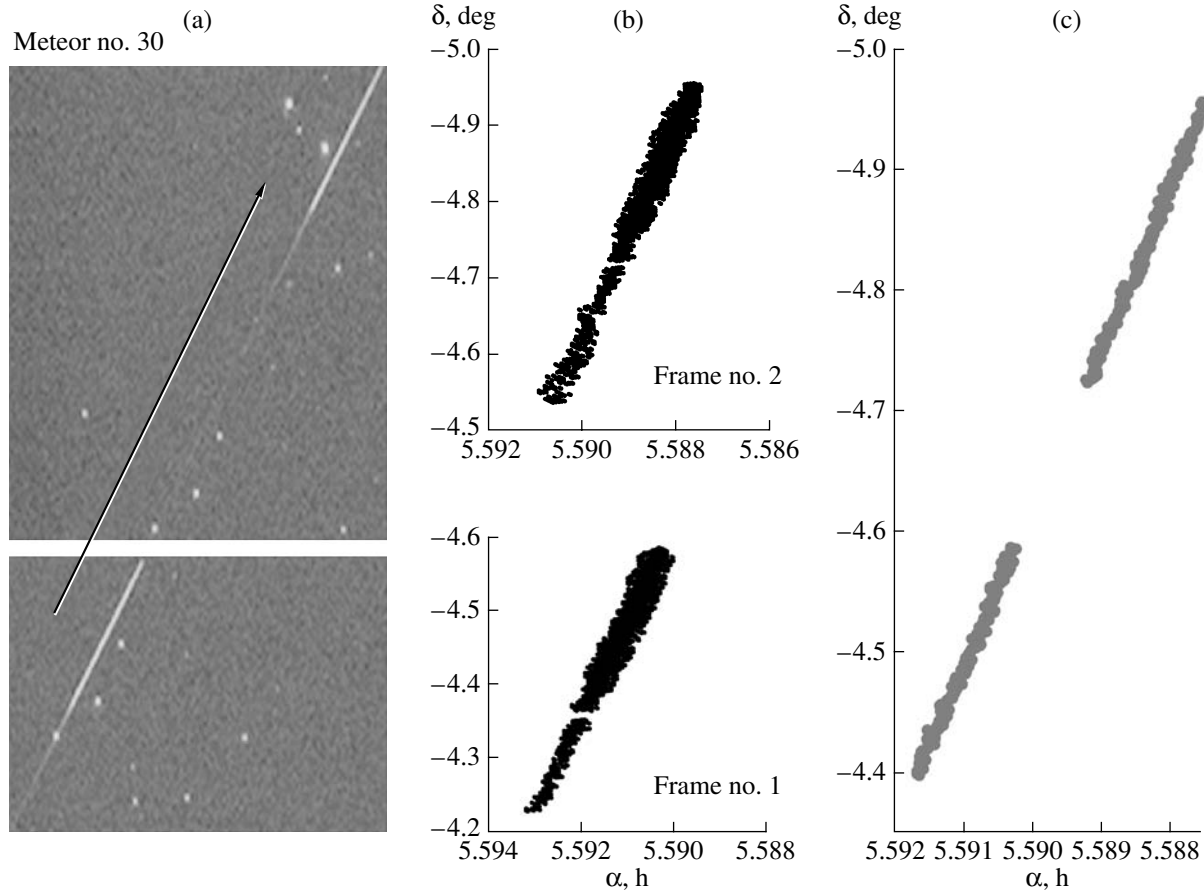


**Fig. 6.** Main meteor image reduction steps: (a) meteor streak images for meteor no. 30 (the arrow indicates the meteor particle flight direction); (b) identification of the meteor image pixels and calculation of their equatorial coordinates; (c) meteor trajectory determination.

Within each such sector, we calculate the  $Y$  coordinate by a weighted averaging of the  $Y$  coordinates of all the image points that fall into a given interval in  $X$  coordinate:

$$\langle Y_i \rangle = \frac{\sum (Y_i I_i)}{\sum I_i}. \quad (3)$$

Thus, the resulting profile is a set of points  $(X_i, \langle Y_i \rangle)$ . The  $Y$  scan is determined in a similar way— $(\langle X_i \rangle, Y_i)$ .

The *meteor image axis* is an average fitting straight line that can represent the meteor trajectory. It can be obtained by iterative approximations. The essence of the method is that the dispersion is calculated at each step for all the meteor image points involved in calculating the straight line, which is used at the next step as a criterion for cutting off random points. Specifying the cutoff level (usually, this is a  $3\sigma$  standard deviation), we can change the noise contribution to the straight-line calculation. The process continues until the standard deviation over the entire working series becomes different from the previous one by a given percent (as a rule,

1%). In the calculations, we clearly see that the ultimate straight line is less distorted by the influence of random points. The change in the coefficients of the straight line during an iteration has the form of a convergent process.

The  $L$  profile is calculated along the meteor trajectory image axis with a given step ( $d_l$ ). This allows the entire image along the meteor axis to be broken down into

$$N = \frac{(L_{\max} - L_{\min})}{d_l}, \quad (4)$$

sectors with width  $d_l$ . Within each such sector, we find the  $D_i$  coordinate as a weighted average of the  $D$  distances of all the points from the meteor trajectory image axis that fall into a given interval in  $D$  coordinate:

$$\langle D_i \rangle = \frac{\sum (D_i I_i)}{\sum I_i}. \quad (5)$$

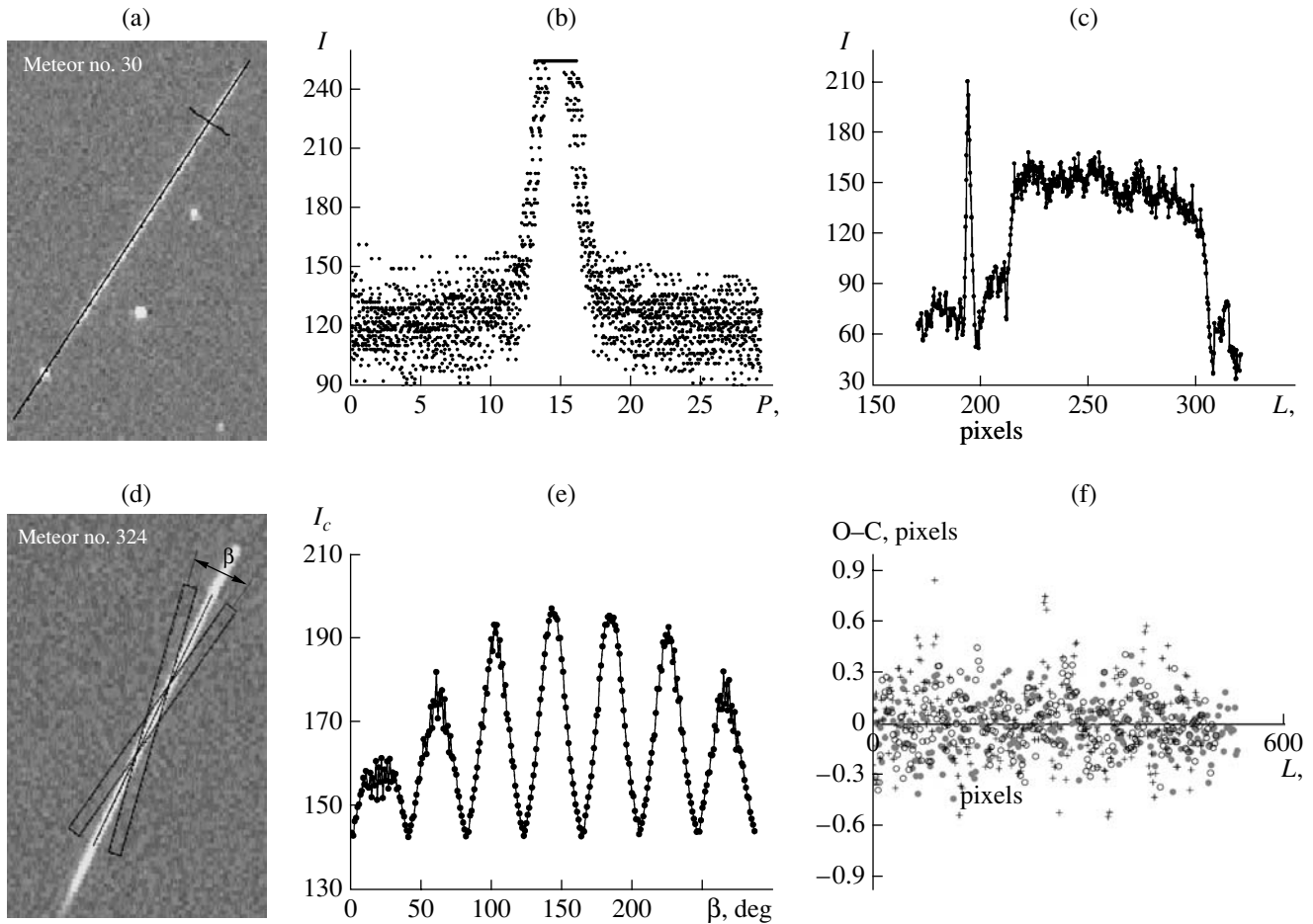


**Fig. 7.** Technique for meteor image measurements: (a) manual drawing of the longitudinal axis of the meteor image and the working window (first approximation); (b) calculation of the integrated transverse scan; (c) calculation of the longitudinal scan, the peak on the left part of the scan belongs to the star image (see Fig. 7a); (d) semiautomatic determination of the longitudinal axis, passage to the coordinate system of the longitudinal axis; (e) dependence of the mean intensity ( $I_c$ ) in the working window on the rotation angle ( $\beta$ ) of the working window relative to the longitudinal axis and the discrete displacements of this window in a direction perpendicular to the longitudinal axis, the maximum corresponds to a larger number of pixels in the working window belonging to the meteor image; (f) deviation of the repeatedly measured points from the axis.

Thus, the resulting profile is a set of points  $(L_i, \langle D_i \rangle)$ , which can be converted to a pair of coordinates in the image frame  $(X_i, Y_i)$  by their transformation from the coordinate system of the meteor image axis.

The corresponding spherical coordinates can be calculated from the measured rectangular coordinates of meteor trajectory points by Turner's method.

Figure 6c presents the results of our meteor image reduction by the described technique.

In the third technique (*PicScan 1.03* software), we tested two approaches to determining the image points belonging to the meteor streak. The first approach is based on the fact that we determine the background intensities using the image pixel intensities before the meteor transit and then assume all of the points with a high intensity to belong to the meteor image. As a rule, during star image photometry, an area near the star is used to choose the background intensities. The meteor

photometry is peculiar in that the background intensities can always be determined in those pixels in which the meteor image was recorded using *background maps*.

This technique allows the images of bright meteors to be unambiguously identified. However, for faint objects, the streak is "ragged" and the identified image depends on the local image background fluctuations. An alternative approach that requires initially passing to the coordinate system associated with the longitudinal axis of the meteor streak image (Fig. 7a) allows these problems to be avoided.

To determine the location of the longitudinal meteor image axis in the zeroth approximation, we specify the location and the working window manually. Subsequently, we calculate the integrated transverse scan in the specified working window (Fig. 7b). By the integrated transverse scan we mean a set of meteor image

points projected onto the axis perpendicular to the trajectory. To refine the location of the longitudinal axis, we must perform additional photometry of the working window. For this purpose, based on the integrated transverse scan, we specify the window boundaries in the coordinate perpendicular to the longitudinal axis.

We will assume all points within the working window to belong to the meteor image and the near-meteor background. This technique allows the images of both bright and faintest meteors to be identified. Subsequently, the refined longitudinal axis is calculated from the working window using the technique of weighted average photometric centers similar to Eq. (1). This technique minimizes the influence of the background in the working window on the axis location.

In addition to the possibility of constructing the transverse scans of meteor images, it is possible to construct the longitudinal scans (Fig. 7c) by this technique, which allows the rectangular coordinates of the meteor streak ends to be measured. A high percentage of meteors have “tails” and the “heads” in bright meteors have a complex structure, which entails an uncertainty in the measurements. By analyzing the signal brightness for the longitudinal scans, we can overcome the uncertainty in measuring the rectangular coordinates of the ends of the meteor streak and tail images. If the meteor image falls on a star image (Fig. 7c), then the distortion of the coordinates of the longitudinal axis will be at its maximum and, hence, the working window is chosen in such a way that the star images do not fall into the working window.

The longitudinal axis of the meteor streak image can also be determined in a semiautomatic mode. During the reduction, the preliminary axis and the working window width are specified in the meteor streak image in the zeroth approximation. For the convenience of our calculations, let us pass to the coordinate system of the longitudinal axis ( $P, \beta$ ). Subsequently, a discrete displacement is made in the working window perpendicular to the axis with some step  $\Delta P$ . For each such point  $P_i$ , the working window rotates (relative to this point) in some specified sector with an angular step  $\Delta\beta$  (Fig. 7d). For each point  $P_i$ , we calculate the mean intensity  $I_c$  of all the pixels that fell into the working window and obtain the dependence of  $I_c$  on the rotation angle  $\beta$  (Fig. 7e). This dependence has a maximum when a larger number of pixels belonging to the meteor image fall into the working window. There exists a value of  $P_i$  at which the meteor image falls entirely into the working window and the pair  $(P_i, \beta_{\max})$  will correspond to the sought-for values.

Based on these values, we calculate the axis parameters, which will be the first approximation. Subsequently, using the new axis, we make a displacement with some step along the axis and calculate the photometric center of the specified meteor image neighborhood for each such point using Eqs. (1). The derived set

of meteor streak image measurements is used to calculate the image axis parameters for the second approximation. The second approximation will suffice to determine the axis with an rms deviation of the measured points from the axis of  $\sim 0.1$  pixel. However, this is the internal error of the method. To determine the actual measurement error, we should measure the meteor streak image many times by varying the working window size,  $\Delta P$ , and  $\Delta\beta$ .

In addition to the scanning technique, an independent technique for adjusting the measuring window position and calculating the location of the longitudinal meteor image axis was developed in the *PicScan 1.03* software. The main measuring window includes two additional windows in each of which the transverse scan of the meteor trajectory image at the streak edges is determined. Manipulating the sizes of the additional windows, the measurer makes the maxima of the transverse meteor streak scans coincident by displacing and rotating the image axis. The meteor trajectory image measurements using the two independent techniques differ by less than 0.2 pixel.

If there is a “hot pixel” or a star image near the meteor streak image (Figs. 7a and 7c), then the nearby points are eliminated from the set of measurements, since these images distort the photometric information about the meteor streak.

Repeated test measurements have shown that the rms deviation of the measured points from the axis for our images increases to 0.2 pixel (Fig. 7f) and corresponds to the accuracy with which the rectangular coordinates of star images are determined (Fig. 3).

The error in the inclination angle of the meteor image axis is  $0.5^\circ$  for bright long meteors and reaches  $1.5^\circ$  for faint, barely discernible meteors.

Since the measurement accuracy depends on the meteor streak length in the image, multiframe images are subjected to the procedure of combining individual images. Based on  $N$  frames, the *Combo 1.02* software produces one combined image that consists of the fragments with meteor trails in a common coordinate system chosen either visually by the operator or by a semiautomatic analysis of the meteor trail profiles in individual frames. Thus, we obtain the image of a unified meteor trajectory that is subjected to reduction.

All of the described techniques are used in meteor streak measurements, depending on the meteor brightness and image equality. The individual measurement error is determined for each image.

#### CALCULATING THE COORDINATES OF THE POLES OF THE GREAT CIRCLES OF METEOR TRAJECTORIES

After the meteor image reduction, we obtain the coordinates of the pole of the great circle of the meteor trajectory using the calculated equatorial coordinates of

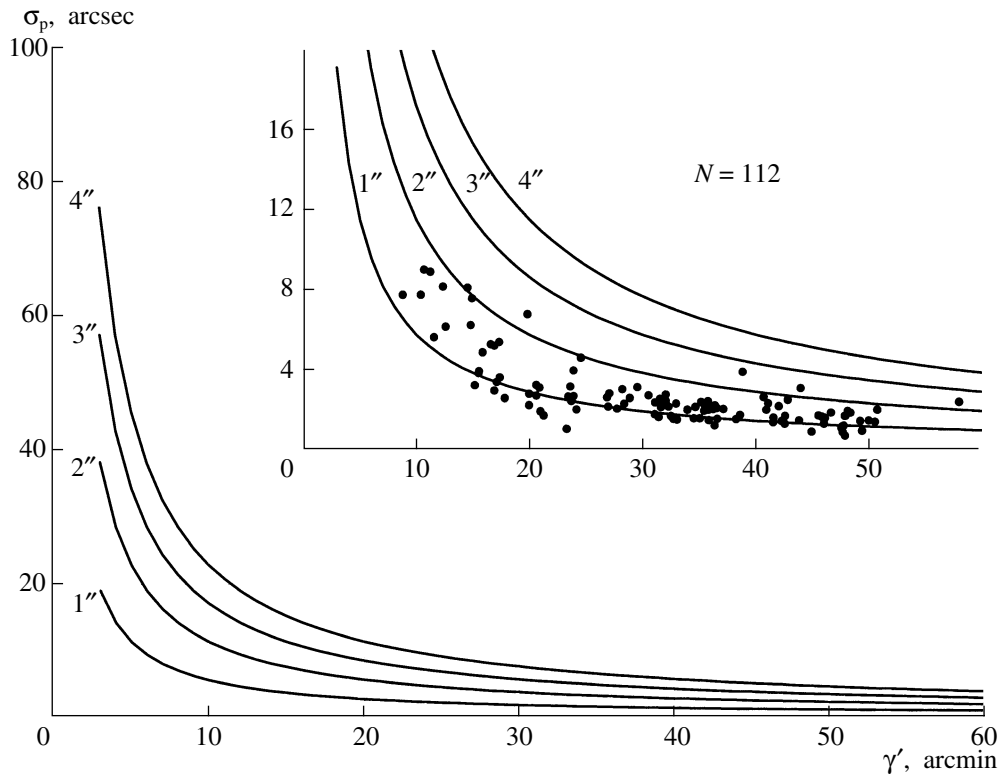


**Fig. 8.** Accuracy of determining the poles of meteor trajectories ( $\sigma$ ) as a function of the arc length ( $\gamma$ ) and the measurement errors (the numbers near the theoretical lines calculated using Eq. (6)). The dots in the inset indicate the actual accuracies of determining the poles of meteor trajectories for randomly chosen 112 meteors.

individual points in the trajectory. In calculating the accuracy of determining the spherical coordinates of the pole of the great circle of the meteor trajectory, we will adhere to the viewpoint (Katasev, 1966) that the error  $\sigma_p$  is defined by

$$\sigma_p = \frac{1}{\sqrt{2}} \frac{\sigma_m}{\sin \gamma}, \quad (6)$$

where  $\gamma$  is the angular length of the meteor trail and  $\sigma_m = \sqrt{\sigma_T^2 + \sigma_t^2}$  is the measurement error in the coordinates of the meteor trajectory points. In our case, the measurement error is determined, first, by the accuracy of measuring the star images by Turner's method,  $\sigma_T$ , and by the accuracy of measuring the meteor trajectory image,  $\sigma_t$ .

Figure 8 presents the dependences of the error in the coordinates of the pole of the great circle of the meteor trajectory on the angular length of its observed fragment (both quantities are in arcminutes). Each dependence was calculated for a certain  $\sigma_m$ , whose value in arcseconds is presented near the corresponding curve. As we see from Fig. 8, the main factor that affects the accuracy of determining the pole coordinates is the meteor trajectory length. For short trajectories (less

than  $10'$ ), this accuracy is more than  $20'$  at a trajectory measurement accuracy of  $4''$ . The meteor trails that were recorded in the TV images in the frame corners and, hence, have small angular lengths are unsuitable for determining the pole coordinates.

Each of these error components,  $\sigma_T$  and  $\sigma_t$ , can vary in some range and produce an error for the measurements of each meteor image. In addition to the theoretical curves at fixed  $\sigma_m$ , the inset in Fig. 8 shows the points calculated for actual meteor images using a sample of 112 meteors. This figure gives an idea of the distribution of measurement errors  $\sigma_m$  whose calculated values lie within the range  $1''$ – $3''$  and, in some fortunate cases, can be less than  $1''$ . As we see from the inset in Fig. 8, if the measurements of the images of meteor trajectories with a length of not less than  $15''$  are used to calculate the pole coordinates, then the error in the pole coordinates  $\sigma_p$  will be less than  $10'$  for the observed meteors even for poorly measurable images with an error of  $4''$ . For reliably measurable images, the errors in the meteor trajectory points is  $1''$ – $2''$ . If the meteor trail was recorded along the image diagonal (in this case, the trajectory length will reach  $60'$ ), then the error in the pole coordinates will be about  $3'$ , which is the limit for our meteor patrol. During the observations, the meteor image can have from 1 to 12 streaks (Fig. 9),

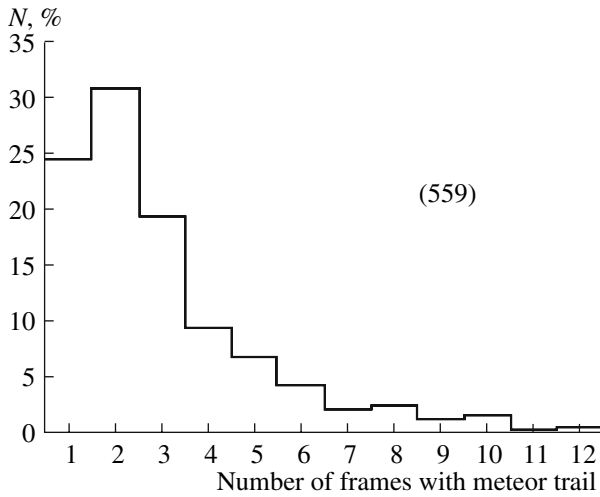


Fig. 9. Histogram of the number distribution of meteor streaks recorded in one movie.

depending on the angular velocity of the meteor and the orientation of its trajectory in the frame. The case of a stationary meteor is also possible. The entire meteor tail then falls into the frame; for example, meteor no. 643 at a length of 20' has 27 streaks. However, stationary meteors are recorded rarely (less than 1% of the entire observational material) and the distribution in Fig. 9 is typical of the overwhelming majority of the observed meteors.

#### CALCULATING THE METEOR RADIANT COORDINATES BY STANYUKOVICH'S METHOD

Calculating the spherical coordinates of radiants generally suggests the existence of meteor images obtained at two basis observing stations and a fortunate location of the basis relative to the meteor trajectory. The case where the angle of approach of the two trajectories is largest is considered a fortunate configuration. Therefore, the accuracy of determining the radiant coordinate decreases with decreasing angle. The radiant coordinates are more difficult to determine from non-basis observations. Stanyukovich (1939) was among the first researchers who developed a technique for such determinations. One of the conditions for the method was the requirement of photographing using an obturator (a rotating sector). In this case, the meteor image was obtained with a series of breaks and there should be at least three such breaks in the image. The method is based on simple relations:

$$\frac{L_m}{L_n} = \frac{\sin \psi_{1n} \sin \psi_{2n} \sin \lambda_m}{\sin \psi_{1m} \sin \psi_{2m} \sin \lambda_n}, \quad (7)$$

where  $L_i$  is the length of any meteor trajectory segment, the alphabetic index points to the number of the meteor path segment, the numerical index indicates its begin-

ning or end,  $\lambda_i$  is the angular length of the segment, and  $\psi_{(1,2i)}$  is the angular distance from the radiant.

For a uniformly rotating obturator sector, the following equality will hold:

$$\frac{L_m}{L_n} = \frac{v_m}{v_n}, \quad (8)$$

where  $v_i$  is the linear velocity in segment  $i$ . If the meteor particle had no deceleration, then the radiant coordinates would be determined quite easily. However, the deceleration cannot be disregarded and Stanyukovich (1939) described a technique for calculating the radiant coordinates and the deceleration using interpolation curves and iterations. As an example, we determined the radiant of a meteor and its relative velocities by this method and compared them with the results of reducing the corresponding observations of this meteor. The difference in declination for the two reduction methods is 24". The above method did not gain acceptance probably due to the complex (for its time) calculation procedure, the requirements to the stability of obturator rotation, and the necessity of using long-focus patrol cameras to increase the spatial resolution.

In our case, Stanyukovich's method gains topicality and can be used along with other methods of radiant coordinate determinations. The focal length of our telescope is 534 mm and the accuracy of determining the beginning and end of the meteor streak is  $\sim 2''$ . As was shown previously (Gorbanev et al., 2006), the frame change accuracy of the patrol TV system is at least 0.1 ms and the timing accuracy deteriorates only due to the existence of tails in meteors. Finally, the current computational power allows any calculations to be easily performed without resorting to simplifications. The amount of observational material suitable for reduction, i.e., when 3 or more full streaks were recorded, accounts of 35% of the total volume (Fig. 9).

Using the main idea of the method, we developed the *FROSA 1.0* software, which allows the right ascension and declination of a meteor radiant to be determined. The calculations consist of the following steps: we select meteors with three or more recorded full streaks, i.e., the coordinates of the beginning and end can be calculated in the streaks. Based on these rectangular coordinates, we determine the corresponding spherical coordinates of the beginning and end of each meteor streak by Turner's method. As the working equation, we use the relations for the right ascension,

$$\frac{\sin(\alpha_R - \alpha_{1n}) \sin(\alpha_R - \alpha_{2n})}{\sin(\alpha_R - \alpha_{1m}) \sin(\alpha_R - \alpha_{2m})} = \frac{v_m \sin(\alpha_{1n} - \alpha_{2n})}{v_n \sin(\alpha_{1m} - \alpha_{2m})}, \quad (9)$$

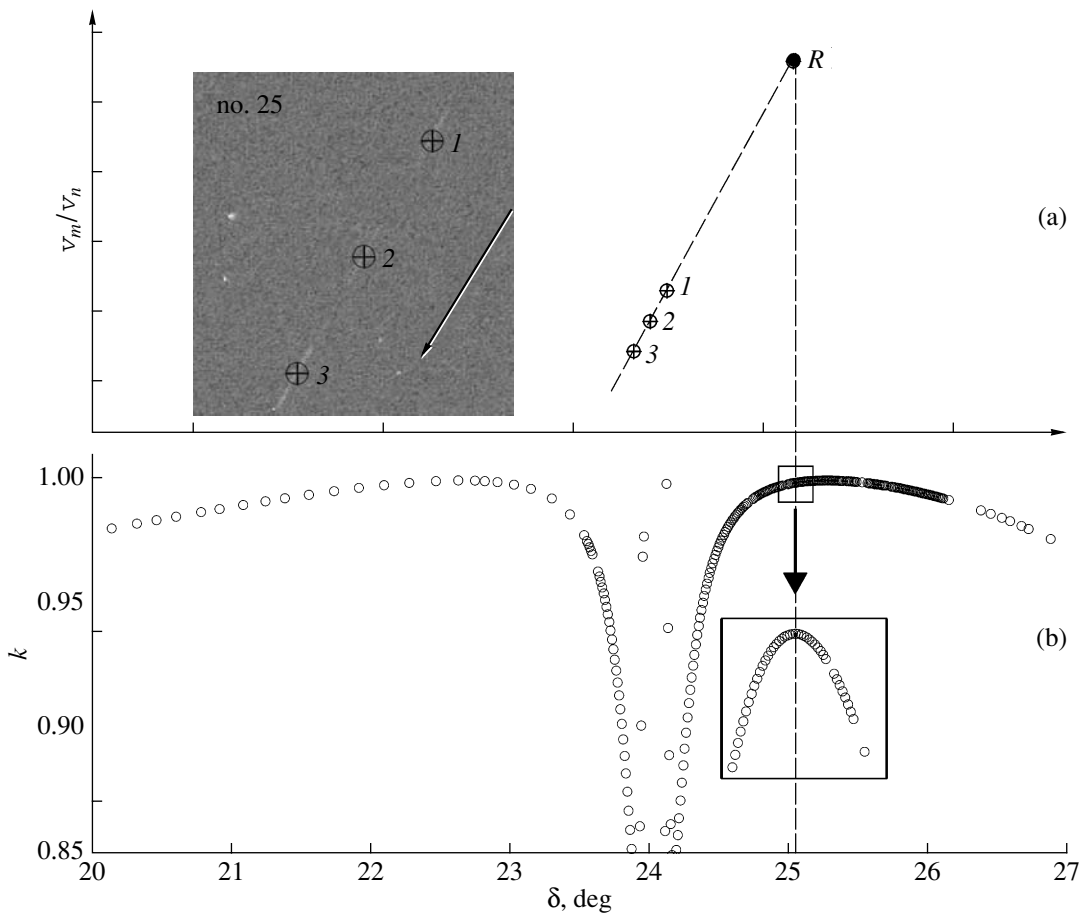


**Fig. 10.** Technique for determining the equatorial coordinates of a meteor radiant by Sanyukovich’s method. The inset shows the combined image of the streaks for meteor no. 25. The numbers in the image and plot (a) denote the streak middle points. The arrow in the inset indicates the meteor particle flight direction. The radiant  $R$  has a declination  $\delta$  (in our example,  $\sim 25^\circ$ ) at which the correlation coefficient  $k$  between the left-hand and right-hand sides of Eq. (10) reaches its maximum for certain  $v_m/v_n$  and  $\delta$ . The right ascension is sought for in a similar way using Eq. (9).

and for the declination,

$$\frac{\sin(\delta_R - \delta_{1n}) \sin(\delta_R - \delta_{2n})}{\sin(\delta_R - \delta_{1m}) \sin(\delta_R - \delta_{2m})} = \frac{v_m \sin(\delta_{1n} - \delta_{2n})}{v_n \sin(\delta_{1m} - \delta_{2m})}, \quad (10)$$

where  $\alpha_R$  and  $\delta_R$  are the right ascension and declination of the radiant;  $\alpha_{ni}$  and  $\delta_{ni}$ s are the right ascension and declination of the beginning ( $n = 1$ ) or end ( $n = 2$ ) of the meteor streak; and  $v$  is the linear velocity of the meteor particle in segment  $i$ .

In meteor astronomy, the meteor images combined from individual images are called velograms. The inset in Fig. 10a presents a fragment of such a velogram for the image of the recorded meteor event with an indication of the flight direction by the arrow and the middle points of the numbered streaks. As an example, Fig. 10a presents the dependence of  $v_m/v_n$  on declination  $\delta$  for

the middle points of the image of three-streak meteor no. 25 (where  $R$  marks the meteor radiant). Using Eq. (10) and varying  $\delta_R$  near the meteor trail, we calculate the corresponding ratios  $v_m/v_n$ . For clarity, we display the points  $(v_m/v_n, \delta)$  in Fig. 10a for the coordinates of the middle points of the meteor streaks and the coordinate of one of the points of the calculated radiant  $R$ . The sought-for point and the middle points of the meteor streaks should lie on the same straight line and for each coordinate  $\delta$  we can calculate the correlation coefficient  $k$  for these points whose maximum value corresponds to the best variant. Figure 10b presents the dependence of the calculated correlation coefficient  $k$  on radiant declination  $\delta$ . The presence of two maxima in this dependence can be explained by the existence of two solutions for Eq. (9) or (10). Therefore, when choosing the radiant coordinate, we should take into account the meteor flight direction. The inset in Fig. 10b presents in more detail the maximum of the dependence  $k(\delta_R)$  corresponding to the sought-for radiant coordi-

nate. It is optimal to perform the iteration process with a variable step in  $\delta_R$  as the maximum is approached.

The radiant point and the meteor trajectory points should lie on the celestial sphere on an arc of the great circle whose equation can be written as

$$\begin{aligned} \operatorname{tg} \delta_1 \sin(\alpha_R - \alpha_2) - \operatorname{tg} \delta_2 \sin(\alpha_R - \alpha_1) \\ = \operatorname{tg} \delta_R \sin(\alpha_1 - \alpha_2), \end{aligned} \quad (11)$$

where  $\alpha_i$  and  $\delta_i$  are the meteor trajectory points.

Having determined the radiant declination, we calculate the corresponding right ascension using Eq. (11).

Similarly, using Eq. (9), we determine the right ascension and then calculate the declination using Eq. (11).

The question arises as to which variant should be used for the meteor being measured. The choice of Eq. (9) or (10) will depend on the orientation of the meteor trajectory on the celestial sphere. If the displacement (in angular units) in right ascension is larger than that in declination, then preference should be given to calculating the right ascension. In this case, the increments in the angular length of meteor streaks calculated in Stanyukovich's method will be determined more reliably.

#### ESTIMATING THE ACCURACY OF CALCULATING THE METEOR RADIANT COORDINATES BY STANYUKOVICH'S METHOD

The error in the radiant coordinates depends on the measurement errors of the beginning and end of the meteor streak,  $\sigma_h$ . The existence of tails in some meteor images affects significantly the measurement accuracy, since their brightness and length more likely reflects the physical rather than kinematic processes. Therefore, meteor streak images with sharp and bright edges are most convenient for measurements. From the standpoint of reliability, the accuracy of measuring the meteor streak head is higher than that for the tail. Therefore, if the meteor event was recorded in the form of an image with six or more streaks but with a tail, then it is better to use only the streak beginning to increase the accuracy.

Since the measurement accuracies for different streaks differ significant, the difficulty in determining the error for the radiant coordinates arises. Therefore, the following technique was used to calculate the error in the radiant coordinates by Stanyukovich's method. For each point of the beginning or end of the meteor streak, we used the individual measurement error obtained from a sample of 30 measurements. Each series of measurements was used to calculate the radiant coordinates by Stanyukovich's method. In this way, we obtained 30 radiant coordinate determinations. In addition, we performed two variants of calculations to

test the assertions about the choice of Eq. (9) or (10) for an individual meteor. For this purpose, using Eq. (9), we determined the right ascension whose value was substituted into Eq. (11) to calculate the corresponding declination. Similarly, we obtain the second pair of radiant coordinates from Eqs. (10) and (11).

Figure 11 presents the results of our reduction of the meteor velogram for meteor no. 35 by Stanyukovich's method. Figure 11a shows the velogram itself and Fig. 11b shows an area of the celestial sphere with the points belonging to the meteor trajectory and the point of the calculated radiant (the arrow indicates the meteor flight direction). The results of our calculations for the two variants are presented in Figs. 11c (the variant of declination calculations based on Eq. (10)) and 11d (the variant of right ascension calculations based on Eq. (9)). As we see from Figs. 11c and 11d, the first variant (the calculations using the equation for the declination) gives errors that are a factor of 2 smaller. Indeed, for meteor no. 35, the angular displacement in declination and right ascension in 0.3 s of its flight are  $\sim 26'$  and  $\sim 17'$ , respectively; i.e., the error of the method is smaller for a larger displacement. This confirms the assertion that the equatorial coordinate for which the meteor streak increment is larger should be used in the calculations for Stanyukovich's method.

The error in determining the radiant coordinates by Stanyukovich's method,  $\sigma_s$ , depends on the error in the pole of the great circle of the meteor,  $\sigma_p$ , and on the measurement error of the coordinates for the meteor streak ends,  $\sigma_h$ . For the right ascension and the declination, we find the errors from the formulas

$$\sigma_s(\alpha) = \sqrt{\sigma_p^2(\alpha) + \sigma_h^2(\alpha)}, \quad (12)$$

$$\sigma_s(\delta) = \sqrt{\sigma_p^2(\delta) + \sigma_h^2(\delta)}. \quad (13)$$

The technique for determining  $\sigma_p$  was described above.

The calculated coordinates of the apparent radiant for meteor no. 35 are  $57^\circ 3' \pm 2'$  in right ascension and  $+22^\circ 54' \pm 3'$  in declination. It should be noted that the calculated quantities are the equatorial coordinates of the apparent radiant referred to the time of observations with the coordinates for the epoch of the Tycho-2 Star Catalogue used. Based on the transit time and the calculated position of the apparent radiant, we can attribute meteor no. 35 to the Northern Taurides ( $58^\circ$ ,  $+22^\circ$ ; the activity time from October 1 to November 25).

Undoubtedly, basis observations give more reliable information on the kinematic characteristics of meteors. At present, we are performing such basis observations, which will be described in the next papers. However, it should be noted that a high percentage of non-basis meteors that can be reduced by the technique

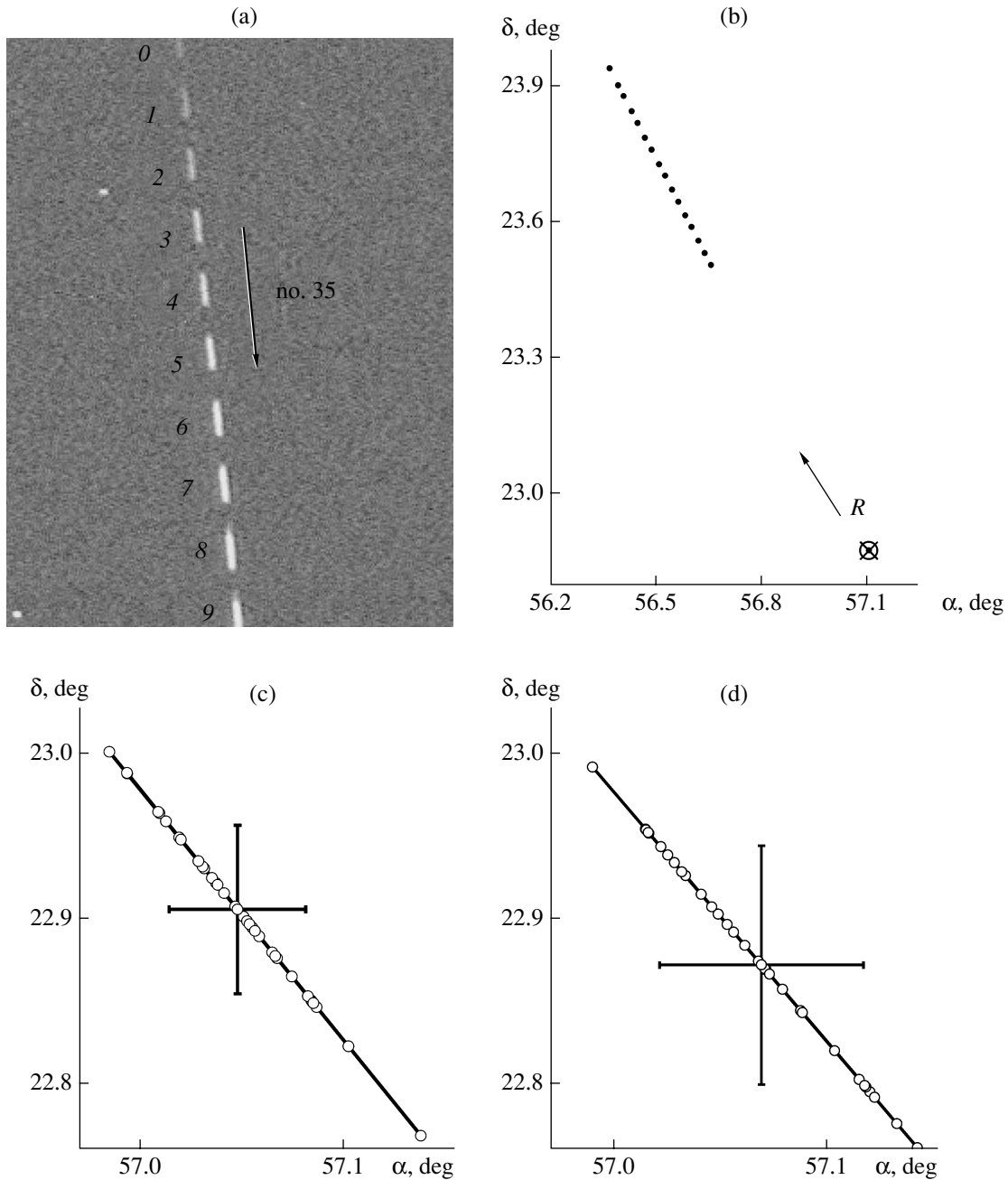


**Fig. 11.** Accuracy of determining the equatorial coordinates of a meteor radiant by Sanyukovich's method: (a) meteor velogram; (b) area of the celestial sphere with the meteor points and the point of the calculated radiant; (c) and (d) on the calculation of the error in the meteor radiant points by the method described in the text.

described above are recorded in the practice of basis meteor observations.

### CONCLUSIONS

Telescopic meteor patrolling using a panoramic TV detector as the recorder along with the possibility of imaging faint meteors with a time resolution of 0.02 or 0.04 s allows the positional measurements to be made

with a hitherto unachievable accuracy. For the images of star-like objects, the positional measurement error is  $\sim 1''$ ; for extended meteor images, this error can be  $1''$  and  $4''$  for bright and faint meteors, respectively. The equatorial coordinates of the poles of the great circles for meteor trajectories can be determined with an error of not worse than  $4'$  for meteor trajectories with a length of at least  $15'$ . Using Sanyukovich's method allows the equatorial coordinates of the radiant to be

determined with an accuracy of at least  $4'-5'$ . The increase in measurement accuracy by an order of magnitude compared to short-focus photographic meteor observations and the time resolution of events allows us to return to the solution of problems in meteor astronomy, whose solution has not been possible previously.

#### REFERENCES

- Behrend, R., Buil, Ch., Antonini, P., and Demeautis, Ch., GSC 628 290: a New EW/KW Variable, *Inform. Bull. Var. Stars*, 2002, no. 5219, p. 1.
- Gehrels, T., Marsden, B.G., and McMillan, R.S., Astrometry with a Scanning CCD, *Astron. J.*, 1986, vol. 91, no. 5, pp. 1242–1243.
- Gorbanev, Yu.M., Golubaev, A.V., Zhukov, V.V., et al., Methods and Statistics of TV Observations of Telescopic Meteors, *Astron. Vestn.*, 2006, vol. 40, no. 5, pp. 449–464 [*Sol. Syst. Res. (Engl. Transl.)*, vol. 40, no. 5, pp. 412–426].
- Katasev, L.A., *Issledovanie meteorov v atmosfere Zemli fotograficheskim metodom* (Investigation of Meteors in the Earth's Atmosphere by Photographic Method), Leningrad: Gidrometeorologicheskoe izd., 1966.
- Kashcheev, B.L. and Lebedinets, V.N., *Radar Observations of Meteors*, Moscow: Akad. Nauk SSSR, 1961, p. 124.
- Kozak, P.N., Analysis of the Methods and Precision of Determination of the Equatorial Coordinates in Digital Reducing of TV Observations of Meteors, *Kinematika Fiz. Nebesnykh Tel*, 2002, vol. 18, no. 5, pp. 471–480.
- Kramer, E.N. and Shestaka, I.S., *Fotograficheskie metody meteornoi astronomii* (Photographic Methods of Meteor Astronomy), Kiev, 1989.
- Nunez, J., Codina, J.M., and Torras, N., Study of the Astrometric Accuracy of Photographic Plates Obtained with Standard Astrographs, *Astron. J.*, 1992, vol. 1-3, no. 5, pp. 1687–1688.
- Martynenko, V.V., Vagner, L.Ya., Kremneva, N.M., et al., Perseid Activity and Radiant Structure in 1972, *Astron. Vestn.*, 1978, vol. 12, no. 4, pp. 235–243 [*Sol. Syst. Res. (Engl. Transl.)*, vol. 12, no. 4, pp. 197–204].
- Mikhailov, A.A., *Kurs obshchei astrofiziki i zvezdnoi astronomii* (A Course of General Astrophysics and Stellar Astronomy), Moscow, 1967.
- Simakina, E.G., Light polarization in the polar regions of Jupiter, *Astron. Vestn.*, 1968, vol. 2, no. 3, pp. 153–157 [*Sol. Syst. Res. (Engl. Transl.)*, vol. 2, no. 3, pp. 115–122].
- Stanyukovich, K.P., Determination of Radiants, Velocities and Altitudes of Meteors from One-Sided Photographs, *Byull. Vsesoyuz. Astron.-Geodez. Obshch.*, 1939, no. 4, pp. 3–1.